Journal of Engineering Mathematics **50:** 329–341, 2004.

Effect of inertia on the Marangoni instability of two-layer channel flow, Part II: normal-mode analysis

M.G. BLYTH and C. POZRIKIDIS[1]

School of Mathematics, University of East Anglia, Norwich, NR4 7TJ, UK (m.blyth@uea.ac.uk); [1]*Department of Mechanical and Aerospace Engineering, University of California, San Diego, La Jolla, California 92093-0411, USA (cpozrikidis@ucsd.edu)*

Received 18 May 2004; accepted in revised form 20 July 2004

Abstract. The effect of inertia on the Yih–Marangoni instability of the interface between two liquid layers in the presence of an insoluble surfactant is assessed for shear-driven channel flow by a normal-mode linear stability analysis. The Orr–Sommerfeld equation describing the growth of small perturbations is solved numerically subject to interfacial conditions that allow for the Marangoni traction. For general Reynolds numbers and arbitrary wave numbers, the surfactant is found to either provoke instability or significantly lower the rate of decay of infinitesimal perturbations, while inertial effects act to widen the range of unstable wave numbers. The nonlinear evolution of growing interfacial waves consisting of a special pair of normal modes yielding an initially flat interface is analysed numerically by a finite-difference method. The results of the simulations are consistent with the predictions of the linear theory and reveal that the interfacial waves steepen and eventually overturn under the influence of the shear flow.

Key words: channel flow, immersed-interface method, Marangoni instability, surfactants

1. Introduction

In a companion article [1], a numerical method was presented for investigating the effect of inertia on the Yih-Marangoni instability of the two-layer channel flow. Results for selected case studies in which either the surfactant concentration or the interface are perturbed from the base-state configuration suggested that the surfactant-induced Marangoni instability persists at non-zero Reynolds numbers, though inertial effects have a mild effect on the growth rates deduced from the amplitude of growing interfacial waves. In this article, these numerical results are put on a rigorous footing by performing a formal normal-mode stability analysis of the two-layer channel flow, accounting for the effect of fluid inertia and surfactant transport.

The stability analysis presented in this article extends a voluminous literature on the Yih interfacial instability in unidirectional viscous flow in the absence of surfactants (*e.g.*, [2]), as well as recent work by Frenkel and Halpern [3,4] and Blyth and Pozrikidis [5] who addressed the problem under the auspices of the lubrication approximation, which is applicable to long waves, and Stokes flow, which is applicable to arbitrary waves. In the presence of fluid inertia, the normal modes are composite eigenfunctions of the Orr–Sommerfeld equation, which is to be solved subject to the usual wall no-slip and no-penetration boundary conditions on the walls, as well as an interfacial condition that accounts for variations in surface tension and Marangoni tractions due to an insoluble surfactant. In the case of Stokes flow, two normal modes arise for a given set of flow conditions: the Yih mode due to viscosity stratification inducing a jump in the interfacial shear, and the Marangoni mode associated with the pres-

ence of the surfactant. In contrast, at finite Reynolds numbers, there is an infinite number of normal modes, and the most dangerous Yih and Marangoni modes are identified by parameter continuation with respect to the Reynolds number.

In Section 2, the linear stability problem is formulated in terms of two companion Orr–Sommerfeld equations for the upper and lower fluid; in Section 3, numerical methods are discussed for solving the generalized eigenvalue problem; in Section 4, the combined effect of fluid inertia and surfactant is illustrated; and in Section 5, the predictions of the linear stability theory are successfully compared with numerical simulations. An overview of the new findings and outlook for further work is presented in the concluding Section 6.

2. Formulation of the linear stability problem

We consider the flow of two adjacent liquid layers in a horizontal channel confined between two parallel walls located at $y=-h_1$, h_2; the unperturbed flat interface is located at $y=0$, as illustrated in Figure 1. By convention, the subscripts 1 and 2 refer to the lower or upper fluid, respectively. The channel walls move in the horizontal direction, x, with velocities U_1 and U_2, generating a Couette-like shear flow in the absence of a streamwise pressure gradient. The interface is occupied by an insoluble surfactant with surface concentration Γ, which is convected and diffuses over the interface, but not into the bulk of the fluids, to locally alter the surface tension, γ. To isolate the effects of surfactant and inertia, we consider fluids with equal densities, whereupon gravity plays no role.

In the base-state undisturbed configuration, the interface is flat, the surfactant concentration is uniform and equal to Γ_0, corresponding to the base-state surface tension γ_0, and the velocity profile is piecewise linear across the channel. To assess the stability of the flow subject to periodic perturbations with wavelength L, we pursue a linear, normal-mode stability analysis. To simplify the calculations, we describe the motion in a frame of reference moving with the interfacial velocity $U_I=(rU_1+\lambda U_2)/(r+\lambda)$, where $\lambda=\mu_2/\mu_1$ is the viscosity ratio, and $r=h_2/h_1$ is the layer thickness ratio.

The flow in both layers is governed by the Navier–Stokes equation and the continuity equation for incompressible fluids, subject to the no-slip and no-penetration condition at the walls. At the interface, the traction undergoes a discontinuity given by

$$\Delta\mathbf{f}\equiv(\boldsymbol{\sigma}^{(1)}-\boldsymbol{\sigma}^{(2)})\cdot\mathbf{n}=\gamma\ \kappa\,\mathbf{n}-\frac{\partial\gamma}{\partial l}\,\mathbf{t}, \tag{2.1}$$

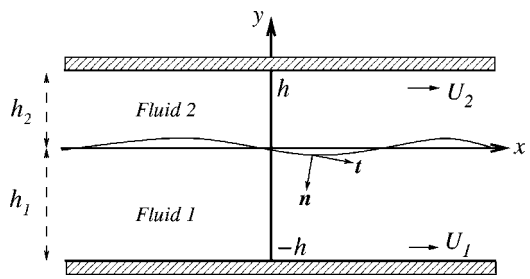

Figure 1. Schematic illustration of two-layer flow in a channel, showing the position of the perturbed interface, described by $y=\eta(x,t)$. The unit vector normal to the interface, **n**, points into the lower fluid 1, and the unit tangent vector, **t**, points in the direction of increasing arc length l. The lower and upper plates move parallel to the x axis with velocities U_1 and U_2.

where $\boldsymbol{\sigma}^{(j)}$ is the Newtonian stress tensor in the jth fluid, $\mathbf{n}$ is the unit normal vector pointing into the lower fluid 1, $\mathbf{t}$ is the unit tangential vector, $\kappa = -\mathbf{n}\cdot \mathrm{d}\mathbf{t}/\mathrm{d}l$ is the interfacial curvature in the xy plane, and l is the arc length increasing in the direction of $\mathbf{t}$.

The surfactant surface concentration $\Gamma(x,t)$, evolves according to the transport equation

$$\frac{\mathrm{d}\Gamma}{\mathrm{d}t} + \frac{\partial(u_t\,\Gamma)}{\partial l} = -\Gamma\,\kappa\,u_n + D_s\frac{\partial^2\Gamma}{\partial l^2}, \tag{2.2}$$

where $u_t = \mathbf{u}\cdot\mathbf{t}$ and $u_n = \mathbf{u}\cdot\mathbf{n}$ are the interfacial velocities in the directions of the tangential and normal vector, respectively, and D_s is the surface surfactant diffusivity (*e.g.*, [6,7]). The derivative $\mathrm{d}/\mathrm{d}t$ on the left-hand side of (2.2) expresses the rate of change of a variable following the motion of interfacial nodes moving with the component of the fluid velocity normal to the interface. Since the surfactant diffusivity is typically small, we take $D_s = 0$ and account for the effect of convection alone.

Next, we introduce dimensionless variables reducing lengths by the lower-layer thickness, h_1, time by the capillary scale $h_1\mu_1/\gamma_0$, pressure by γ_0/h_1, the surfactant concentration by Γ_0, and the surface tension by γ_0, where μ_1 is the lower-fluid viscosity. Henceforth, all variables will be tacitly assumed to be dimensionless according to this convention.

In the lower layer extending over $-1 \le y \le 0$, the base-state x and y velocity components are given by $u_1^{(0)} = sy$, $v_1^{(0)} = 0$; in the upper layer, extending over $0 \le y \le r$, the velocity components are $u_2^{(0)} = (s/\lambda)y$, $v_2^{(0)} = 0$, where

$$s \equiv \frac{\mu_1}{\gamma_0}\frac{\lambda}{\lambda + r}\,(U_2 - U_1)\,, \tag{2.3}$$

is the dimensionless interfacial shear rate of the lower fluid, playing the role of a capillary number.

The formulation of the linear stability problem at hand was discussed in detail by Frenkel and Halpern [3,4]. In the remainder of this section, we recapitulate the basic formulation and state the governing equations.

A perturbation displaces the otherwise flat interface to a position described by $y = \eta(x,t)$, where $|\eta|$ is assumed to be small. In the case of a normal-mode disturbance with wave number k, the waveform of the interfacial elevation is $\eta(x,t) = A_1\exp(\mathrm{i}k[x-ct])$, where A_1 is a complex amplitude and $c = c_r + \mathrm{i}c_i$ is the complex wave speed. The stream function, pressure, and surfactant concentration are expressed in the corresponding forms

$$\Big(\psi_j,\ p_j,\ \Gamma\Big) = \Big(\psi_j^{(0)},\ p^{(0)},\ \Gamma_0\Big) + \Big(\psi_j^{(1)}(y),\ p_j^{(1)}(y),\ \Gamma_1\Big)\,\exp(\mathrm{i}k[x-ct]), \tag{2.4}$$

where $j = 1, 2$ refers to fluids 1 and 2 respectively. The disturbance streamfunction, $\psi_j^{(1)}$, is defined so that the x and y velocity components in the jth fluid derive from the usual relations $u_j^{(1)} = \partial\psi_j^{(1)}/\partial y$ and $v_j^{(1)} = -\partial\psi_j^{(1)}/\partial x$. Substituting (2.4) in the non-dimensionalized Navier–Stokes equation and linearizing, we arrive at the standard Orr–Sommerfeld equation. In dimensionless form, this reads

$$\lambda_j\Big(\frac{\mathrm{d}^2}{\mathrm{d}y^2} - k^2\Big)^2\psi_j^{(1)} = \mathrm{i}k\frac{\mathrm{Re}}{\mathrm{Ca}}\Big[\,(u_j^{(0)} - c)\Big(\frac{\mathrm{d}^2}{\mathrm{d}y^2} - k^2\Big)\psi_j^{(1)} - \psi_j^{(1)}\,\frac{\mathrm{d}^2u_j^{(0)}}{\mathrm{d}y^2}\,\Big], \tag{2.5}$$

where $\lambda_1 = 1$, $\lambda_2 = \lambda$, $\mathrm{Re} = \rho V h_1/\mu_1$ is the Reynolds number, $\mathrm{Ca} = \mu_1 V/\gamma_0$ is the capillary number, and V is an appropriate reference velocity. The ratio Re/Ca on the right-hand side of (2.5) is equal to $\rho h_1\gamma_0/\mu_1^2$, independent of V. When $U_2 > U_1$, it is physically meaningful to

define $V = U_I - U_1$, whereupon Ca reduces to the dimensionless shear rate, s, defined in (2.3). This choice will be tacitly assumed in the remainder of our discussion.

Linearizing the kinematic condition at the interface, $\mathrm{D}[y - \eta(x,t)]/\mathrm{D}t = 0$, where $\mathrm{D}/\mathrm{D}t$ is the material derivative, we find $A_1 = \psi_1^{(1)}(0)/c$. Requiring that the velocity is continuous across the interface yields the conditions

$$\psi_1^{(1)}(0) = \psi_2^{(1)}(0), \qquad \lambda\Big(\frac{\mathrm{d}\psi_1^{(1)}}{\mathrm{d}y} - \frac{\mathrm{d}\psi_2^{(1)}}{\mathrm{d}y}\Big)_{y=0} = \frac{s}{c}(1-\lambda)\,\psi_1^{(1)}(0), \tag{2.6}$$

where a prime indicates differentiation with respect to y. Linearizing the normal component of the interfacial force balance (2.1) and eliminating the interfacial pressures using the x component of the momentum equation, we obtain

$$\lambda\Big(\frac{\mathrm{d}^3\psi_2^{(1)}}{\mathrm{d}y^3} - 3k^2\frac{\mathrm{d}\psi_2^{(1)}}{\mathrm{d}y}\Big)_{y=0} - \Big(\frac{\mathrm{d}^3\psi_1^{(1)}}{\mathrm{d}y^3} - 3k^2\frac{\mathrm{d}\psi_1^{(1)}}{\mathrm{d}y}\Big)_{y=0} = -\mathrm{i}\frac{k^3}{c}\,\psi_2^{(1)}(0). \tag{2.7}$$

Linearizing the transport Equation (2.2), we obtain an expression for the surfactant concentration eigenfunction,

$$c\Gamma_1 = \Big(\frac{\mathrm{d}\psi_1^{(1)}}{\mathrm{d}y} + \frac{s}{c}\,\psi_1^{(1)}\Big)_{y=0}. \tag{2.8}$$

Substituting this expression in the tangential component of the interfacial stress balance, we find

$$\lambda\Big(\frac{\mathrm{d}^2\psi_2^{(1)}}{\mathrm{d}y^2} + k^2\psi_2^{(1)}\Big)_{y=0} - \Big(\frac{\mathrm{d}^2\psi_1^{(1)}}{\mathrm{d}y^2} + k^2\psi_1^{(1)}\Big)_{y=0} = \mathrm{i}Ma\,\frac{k}{c}\Big(\frac{\mathrm{d}\psi_1^{(1)}}{\mathrm{d}y} + \frac{s}{c}\psi_1^{(1)}\Big)_{y=0}, \tag{2.9}$$

where $\mathrm{Ma} = E\Gamma_0/\gamma_0$ is the Marangoni number, and E is the surface elasticity defined from the linear interface constitutive equation $\gamma = \gamma_0 - E(\Gamma - \Gamma_0)$. Finally, to satisfy the no-slip and no-penetration conditions at the upper and lower walls, we require

$$\psi_1^{(1)}(-1) = \Big(\frac{\mathrm{d}\psi_1^{(1)}}{\mathrm{d}y}\Big)_{y=-1} = \psi_2^{(1)}(r) = \Big(\frac{\mathrm{d}\psi_2^{(1)}}{\mathrm{d}y}\Big)_{y=r} = 0. \tag{2.10}$$

The task now is to solve the two Orr–Sommerfeld equation (2.5) in each fluid, subject to conditions (2.6–2.10). The complex phase velocity of a perturbation depends on the reduced wave number, k, viscosity ratio, λ, layer depth ratio, r, shear parameter s or capillary number Ca, Reynolds number, Re, and Marangoni number Ma.

3. Numerical methods

The Orr–Sommerfeld equation (2.5) accompanied by the boundary conditions (2.6–2.10) was solved numerically using a Chebyshev tau method (*e.g.*, [8,9]). To implement the method, we map each of the two fluid regions $-1 \le y \le 0$ and $0 \le y \le r$ onto the standard interval $-1 \le y_j \le 1$, for $j = 1, 2$, writing

$$y_1 = 2\Big(y + \frac{1}{2}\Big) \quad \text{in fluid 1,} \qquad y_2 = \frac{2}{r}\Big(y - \frac{r}{2}\Big) \quad \text{in fluid 2.} \tag{3.1}$$

Next, we expand the stream function within each fluid in a truncated series of Chebyshev polynomials, $T_k(y_j)$, by setting

$$\psi_j^{(1)}(y_j) = \sum_{k=0}^{N_j} a_{jk}\,T_k(y_j), \tag{3.2}$$

for $j=1,2$, where a_{jk} are unknown coefficients, and N_1, N_2 are specified truncation levels for each layer. Substituting (3.2) in (2.5) for $j=1,2$, and projecting the resulting equations onto $T_m(y_j)$ for $m=0,\ldots N_j-4$ under the Chebyshev inner product,

$$\langle T_m(x),\, f(x)\rangle = \int_{-1}^{1} \frac{1}{\sqrt{1-x^2}}\, T_m(x) f(x)\, \mathrm{d}x, \tag{3.3}$$

we derive a system of N_1+N_2-6 equations for the N_1+N_2+2 coefficients a_{jk}. All integrals involving Chebyshev polynomials and their derivatives in the projection may be computed exactly using known identities and recursive relations (*e.g.*, [10, pp. 159–161]). A further set of 8 equations are obtained by substituting (3.2) in the boundary conditions (2.6–2.10). To simplify the calculation, the quadratic in c term in the tangential condition (2.9) is eliminated by substituting for $\psi_1^{(1)}(0)$ using the second equation in (2.6).

The complete set of equations is finally assembled into the linear system

$$\mathbf{A}\cdot\mathbf{w} = c\,\mathbf{B}\cdot\mathbf{w}, \tag{3.4}$$

where $\mathbf{w}=(a_{10},\ldots,a_{1N_1},a_{20},\ldots,a_{2N_2})^T$, and $\mathbf{A}$, $\mathbf{B}$ are square matrices of linear size N_1+N_2+2. The generalized eigenvalue problem expressed by (3.4) was solved using a NAG routine based on the QZ algorithm to obtain the complex phase velocity, c, and thus extract the growth rate, $\sigma = kc_i$. To filter out spurious eigenmodes, the truncation levels N_1 and N_2 are increased until genuine modes are clearly identified. Typically, $N_1=N_2=25$ terms are sufficient to obtain a good level of accuracy at small and moderate Reynolds numbers. However, larger values are required to accurately resolve the eigenfunctions at high Reynolds numbers. For example, when $\mathrm{Re}=1{,}000$ it is necessary to take $N_1=N_2=45$.

A first check of the accuracy of the numerical method was performed by comparing the present results with available results for the plane Couette flow of a homogeneous fluid (*e.g.*, [11]), and confirming excellent agreement. A further check was performed by comparing the growth rates of the two-layer channel flow with those obtained by an alternative shooting method based on fourth-order Runge–Kutta integration (*e.g.*, [12, p. 452]). In this method, an initial guess is made for c, and the Orr–Sommerfeld equation in the lower fluid is integrated forward from $y_1=-1$, corresponding to the lower wall, to $y_1=1$, corresponding to the interface. The integration in the upper fluid is then initialized at $y_2=-1$, with starting values provided by the interfacial boundary conditions (2.6–2.9), and continued up to $y_2=1$. An updated value of c is calculated using Newton's method and the procedure is iterated until convergence is achieved to within a prescribed tolerance. Excellent agreement was found between the two numerical procedures at low Reynolds numbers, providing further assurance that only genuine eigenmodes are retained in the solution of (3.4). At higher Reynolds numbers, the shooting method falters as boundary layers arise. In contrast, accurate solutions with the Chebyshev tau method can be obtained without difficulty at high Reynolds numbers.

To gain further confidence in the spectral code, growth rates were computed for an interface that is devoid of surfactants, $\mathrm{Ma}=0$. According to Yih's [13] long-wave analysis, when $k\mathrm{Re}$ is small, $c_i \simeq k\mathrm{Re}J/(\lambda\mathrm{Ca})$ where the group J is defined by a lengthy expression. With $r=1$, $\lambda=0{\cdot}1$, $s=\mathrm{Ca}=1/11$, $J=4\times10^{-4}$, in Figure 2 we plot c_i for the most dangerous mode against $k\mathrm{Re}/(\lambda\mathrm{Ca})$, together with a straight line of slope 4×10^{-4} passing through the origin. The excellent agreement with Yih's approximate result near the origin confirms the accuracy of the numerical code. We note, in particular, that instability at the interface arises only in the presence of fluid inertia.

Renardy [14] investigated the stability of the two-layer flow in the absence of surfactants, and compared her results with the earlier results of Hooper and Boyd [15] for a sheared

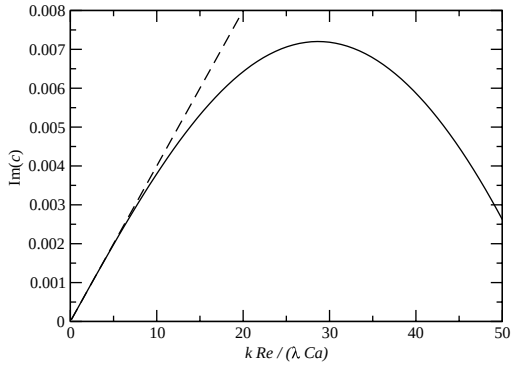

Figure 2. Comparison of the present results for arbitrary wave numbers with Yih's results for long waves on a clean interface for $r=1$, $\lambda=0{\cdot}1$, $s=\mathrm{Ca}=1/11$, and $\mathrm{Ma}=0$. The solid line corresponds to the present numerical results, and the broken line is Yih's long-wave approximation, $c_i \simeq 4\times 10^{-4}\, k\mathrm{Re}/(\lambda\mathrm{Ca})$.

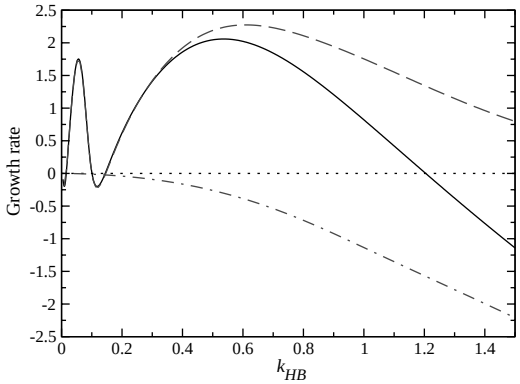

Figure 3. Graph of the growth rate kc_i versus wave number k_{HB} for $\lambda=2{\cdot}0$, $r=2{\cdot}0$, $\mathrm{Re}=133{\cdot}0$, and $s=\mathrm{Ca}=115{\cdot}725$. The solid line is for $\mathrm{Ma}=0$, and the broken and dot-dashed lines are, respectively, for the first and second modes when $\mathrm{Ma}=0{\cdot}1$.

interface between two unbounded fluids. As the separation between the upper and lower walls increases, a band of unstable wave numbers eventually appears, matching a band identified by Hooper and Boyd [15] in the absence of confining walls. Our results are in excellent agreement with those shown in Figure 1 of Renardy [14] for a clean interface and parameter values $\lambda=2{\cdot}0$, $r=2{\cdot}0$, $\mathrm{Re}=133{\cdot}0$, $s=\mathrm{Ca}=115{\cdot}725$ and $\mathrm{Ma}=0$, corresponding to Renardy's alternative Reynolds number $\mathrm{Re}_1=798{\cdot}0$. Under the implicit assumption that the velocity scale is $V=U_I-U_1$, Re_1 is related to our Reynolds number by $\mathrm{Re}=\lambda\mathrm{Re}_1/[(\lambda+r)(1+r)]$. The reduced growth rate, kc_i, is shown with the solid line in Figure 3. Note that for ease of comparison with Renardy's [14] Figure 1, the scaled wave number, k_{HB}, was adopted as the ordinate, where $k_{HB}=k/\mathrm{Re}^{1/2}$. In particular, the boundaries between stable and unstable wave numbers coincide with those presented in Renardy's figure.

4. Results and discussion

Precisely two normal modes arise under conditions of Stokes flow: the Marangoni mode associated with the presence of the surfactant, and the Yih mode associated with an interface free of contaminants. A clean interface is always stable, whereas a contaminated interface becomes unstable over a certain range of parameter values. When inertia is present, there is an infinite

number of normal modes; lowering the Reynolds number in a continuous manner allows us to identify the Yih and Marangoni modes.

The effect of surfactants in the presence of fluid inertia is demonstrated by the broken and dot-dashed lines in Figure 3, corresponding to the two most dangerous modes for $\mathrm{Ma} = 0{\cdot}1$. It is interesting that the dashed line virtually lies on top of the solid line all the way up to $k_{HB} \simeq 0{\cdot}3$, so the surfactant has little effect on the growth rate of the Yih mode. However, in the narrow window of stable wave numbers around $k_{HB} = 0{\cdot}12$, the growth rate of the second mode, represented by the dot-dashed line, is significantly higher than that in the absence of surfactant. Over this narrow range, the surfactant noticeably reduces the rate at which small perturbations decay. When $\mathrm{Ma} = 0$, the flow is stable to wave numbers above a critical value $k_{HB}^{c} \approx 1{\cdot}2$. This critical threshold increases when surfactant is introduced; accordingly, the dashed line crosses the axis at a higher wave number. Large values of Re_1 correspond to a large separation between the upper and lower walls, permitting comparison with the predictions for unbounded flow studied by Hooper and Boyd [15]. For a contaminated interface, the increase in the critical value k_{HB}^{c} may indicate a similar broadening of the unstable range of wave numbers in the case of unbounded flow.

Figure 4 shows the neutral stability curve in the (Re, k) plane for $\mathrm{Ma} = 1{\cdot}0$, $r = 2{\cdot}0$, $\lambda = 0{\cdot}5$, and $s = 2$ corresponding to $\mathrm{Ca} = 2{\cdot}0$. Previous stability analysis for Stokes flow has revealed that introducing a surfactant opens up a range of unstable wave numbers extending from zero up to the critical cut-off value $k_{\mathrm{crit}} = 1{\cdot}65$. The results shown in Figure 4 demonstrate that inertial effects act to widen the range of unstable wave numbers. Moreover, at the critical value $\mathrm{Re}_{\mathrm{crit}} = 12{\cdot}63$, a second small window of stable wave numbers appears, extending upwards in Re to form an island of stable modes, with the island nose located at $(\mathrm{Re}_{\mathrm{crit}}, k_{\mathrm{crit}}) = (12{\cdot}63, 0{\cdot}37)$.

To examine the origin of the stable loop as Re passes through $\mathrm{Re}_{\mathrm{crit}}$, in Figure 5 we plot the growth rates of the two most unstable modes against the Reynolds number, up to and beyond $\mathrm{Re}_{\mathrm{crit}}$, for $k = 0{\cdot}37$, corresponding to the stable island nose. At $\mathrm{Re} = 0$, linear stability for Stokes flow predicts the growth rates $-0{\cdot}0955$ and $0{\cdot}0479$, respectively, for the Yih and Marangoni mode. The present results show that the Marangoni mode remains dominant over the range of Reynolds numbers considered, and passes through zero at $\mathrm{Re} = 12{\cdot}63$ to inaugurate the stable loop.

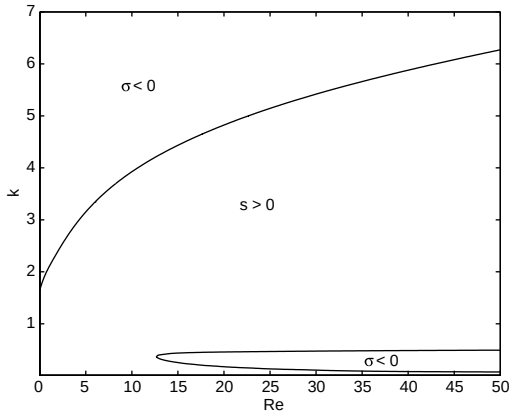

Figure 4. Neutral stability curves separating stable from unstable wave numbers for $\mathrm{Ma} = 1{\cdot}0$, $r = 2{\cdot}0$, $\lambda = 0{\cdot}5$, and $s = \mathrm{Ca} = 2{\cdot}0$.

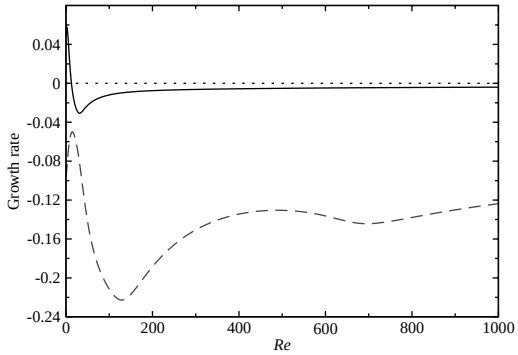

Figure 5. Effect of Re on the growth rate of the Yih mode (broken line) and Marangoni mode (solid line) for $k = 0{\cdot}37$, $\mathrm{Ma} = 1{\cdot}0$, $r = 2{\cdot}0$, $\lambda = 0{\cdot}5$, and $s = \mathrm{Ca} = 2{\cdot}0$.

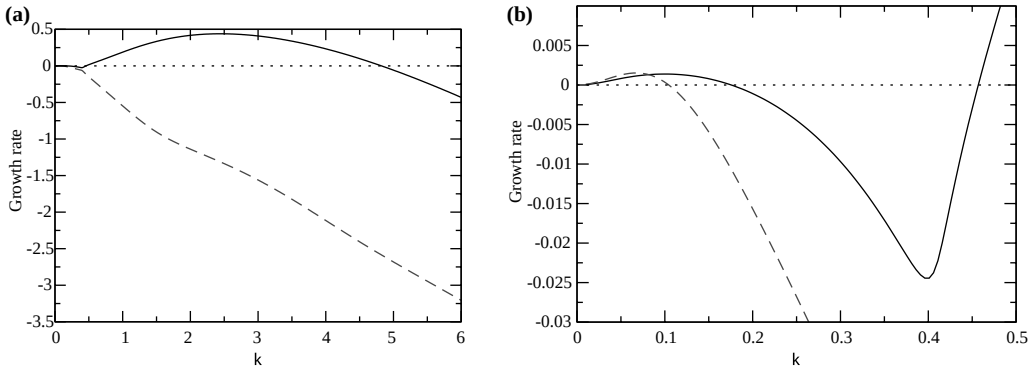

Figure 6. Dependence of the growth rate on the wave number for the Yih mode (broken line) and Marangoni mode (solid line), for $\mathrm{Re} = 20{\cdot}0$, $\mathrm{Ma} = 1{\cdot}0$, $r = 2{\cdot}0$, $\lambda = 0{\cdot}5$, and $s = \mathrm{Ca} = 2{\cdot}0$. (*b*) Close-up of (*a*) near $k = 0$.

Figure 6 illustrates the dependence of the growth rates of the Yih and Marangoni modes on the wave number, for a fixed Reynolds number $\mathrm{Re} = 20{\cdot}0$. The close-up near $k = 0$, presented in Figure 6(*b*), shows that the Yih mode dominates up to $k = 0{\cdot}082$. Beyond this value, the overall stability of the two-layer flow is determined by the Marangoni mode. In particular, the solid line crosses below the wave number axis at $k \approx 0{\cdot}18$ and re-crosses it at $k \approx 0{\cdot}46$, producing a short range of small stable wave numbers. A much longer period of unstable modes follows before the solid line once more crosses the axis at $k \approx 4{\cdot}82$. These results clearly demonstrate the crucial role of the surfactant. For general combinations of the Reynolds number and wave number, the surfactant either provokes instability or significantly lowers the rate of decay of infinitesimal perturbations.

Blyth and Pozrikidis [5] observed that, under conditions of Stokes flow and when the undisturbed interface lies midway between the channel walls, the two-layer flow is stable to small wavelength perturbations. Yih's results show that under the same conditions, perturbations of sufficiently small wave number in the absence of surfactant grow for all Reynolds numbers. The neutral curve shown in Figure 7 indicates that, when $r = 1$ and with both inertia and surfactant present, the flow is unstable to small wave number perturbations. However, beyond the critical Reynolds number $\mathrm{Re} \approx 4{\cdot}8$, the growth rate is negative for a small band of wave numbers subtended from zero to a critical value, so that small wave number disturbances are stabilized by the surfactant.

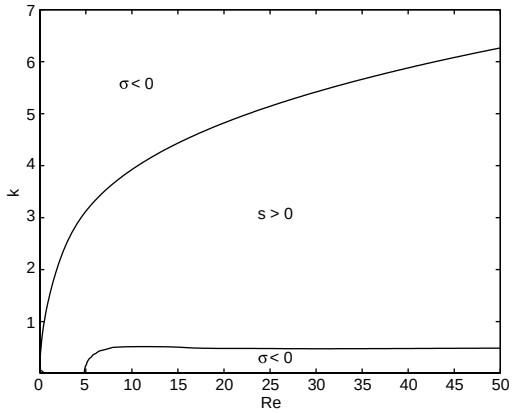

Figure 7. Neutral stability curve for layers of equal thicknesses, $r = 1$, and $\mathrm{Ma} = 1{\cdot}0$, $\lambda = 0{\cdot}5$ and $s = \mathrm{Ca} = 2{\cdot}0$. Since the flow is stable at $\mathrm{Re} = 0$, the upper curve approaches the origin.

Halpern and Frenkel [4] noted that, at zero Reynolds number, the Yih and Marangoni modes both have negative growth rates when the viscosity ratio is increased beyond $\lambda \approx r^2$. Raising λ towards this value for arbitrary Reynolds numbers, we find a significant change in the topology of the neutral stability curve. In particular, the upper curve bulges outwards close to $\mathrm{Re} = 0$, while the lower stable region extends to the left until, eventually, the two make contact at a point, as shown in Figure 8. Thereafter, as λ is raised, the two curves split apart leaving an island of unstable modes around the origin, which is separated from a much larger hoop of unstable modes to the right. The island of unstable modes shrinks as λ is raised further, and ultimately disappears at $\lambda \approx 4{\cdot}0 = r^2$.

5. Numerical simulation of the finite-amplitude motion

In Part I [1], a numerical method was implemented to describe the non-linear stages of the instability beyond the confines of linear stability. The algorithm combines Peskin's immersed-interface method with the diffuse-interface approximation, wherein the step discontinuity in the fluid properties is replaced by a transition zone defined in terms of a mollifying function. A finite-difference method is used to integrate the generalized Navier–Stokes equation

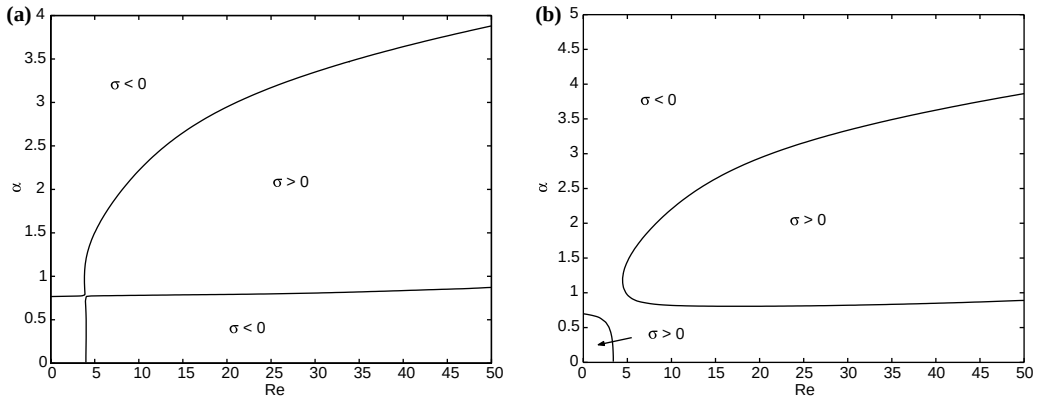

Figure 8. Neutral stability curves for $\mathrm{Ma} = 1{\cdot}0$, $r = 2{\cdot}0$, $s = \mathrm{Ca} = 2{\cdot}0$ and (*a*) $\lambda = 3{\cdot}15778$ and (*b*) $\lambda = 3{\cdot}25$.

incorporating the jump in the interfacial traction, and a finite-volume method is used to solve the surfactant transport equation along the evolving interface.

In the numerical simulations, it is desirable to begin with an initial condition where the interface is flat, and the perturbation is introduced by disturbing the surfactant concentration, the flow, or both. Unfortunately, this initial condition is inconsistent with a monochromatic normal-mode perturbation, which requires a non-zero initial interfacial and surfactant concentration amplitude, both growing at an exponential rate at subsequent times. In particular, the domain perturbation embedded in the linear stability analysis to transfer the matching conditions from the perturbed to the unperturbed interface position frustrates the initialization of the velocity field at the finite-difference nodes near the interface.

To overcome this difficulty, we use an initial condition that is composed of a linear combination of two monochromatic normal modes, one associated with the Yih instability, and the second associated with the Marangoni instability. In the two-mode perturbation, the initial interfacial shape and perturbation in the surfactant concentration are given by the real parts of

$$y(x) = \epsilon \left(A_1 - w\, A_2 \right) \exp(\mathrm{i}kx), \qquad \Gamma^{(1)}(x) = \epsilon \left(\Gamma_1 - w\, \Gamma_2 \right) \exp(\mathrm{i}kx), \tag{5.1}$$

where the subscript 1 or 2 denotes the first or second normal mode, and w is an arbitrary parameter determining the relative weight of the two modes. Without loss of generality, we may assume that the interface amplitudes A_1 and A_2 are real. The corresponding perturbation streamfunction is given by

$$\psi^{(1)}(x, y) = \epsilon \left(f_1(y) - w\, f_2(y) \right) \exp(\mathrm{i}kx), \tag{5.2}$$

where the eigenfunctions $f_1(y)$ and $f_2(y)$ arise by solving the Orr–Sommerfeld Equation. To obtain an initially flat interface, we set $w = A_1/A_2$. With this choice, the initial surfactant concentration is given by

$$\Gamma^{(1)}(x) = \epsilon\, A_1 \left(\beta_1 - \beta_2 \right) \exp(\mathrm{i}kx), \tag{5.3}$$

where $\beta_1 \equiv \Gamma_1/A_1$ and $\beta_2 \equiv \Gamma_2/A_2$ are the complex amplitude ratios.

As a first test case, we consider a two-layer flow with $r = 2$, $\lambda = 1$, $\mathrm{Ca} = 2$, $\mathrm{Re} = 1{\cdot}333$, and $\mathrm{Ma} = 1{\cdot}0$, and compute the evolution of a perturbation with wave number $k = 2\pi/9$. Under these conditions, the Yih normal mode decays with dimensionless rate -0.214921, whereas the Marangoni normal mode grows with dimensionless rate $0{\cdot}097853$. Figure 9(*a*) illustrates the structure of the initial velocity field corresponding to the two-mode perturbation. The sinusoidal curves represent the predicted position of the interface at times $t = 0$ (flat), 10, 20, and 30, for initial amplitude in the surfactant concentration $0{\cdot}10$. Note that in this figure x and y are dimensional variables reduced by the disturbance wavelength L.

The solid lines in Figure 9(*b*) represent the results of the numerical simulation, and the broken lines represent the predictions of linear theory at a sequence of time intervals $t = 0, 1, 2, \ldots$. The agreement between the numerical and theoretical predictions is excellent in the early stage of the motion. Both show that the nodes of the developing interfacial wave drift along the x axis due to the different phase velocity of the two components of the bimodal initial perturbation. Moreover, the simulation reveals that the growing sinusoidal wave tends to steepen under the action of the shear flow. Figure 9(*c*) describes the nonlinear stages of the instability leading to the development of a saw-tooth interfacial profile. At long times, the interface tends to overturn, as wisps of the upper fluid penetrate the lower fluid, and vice versa.

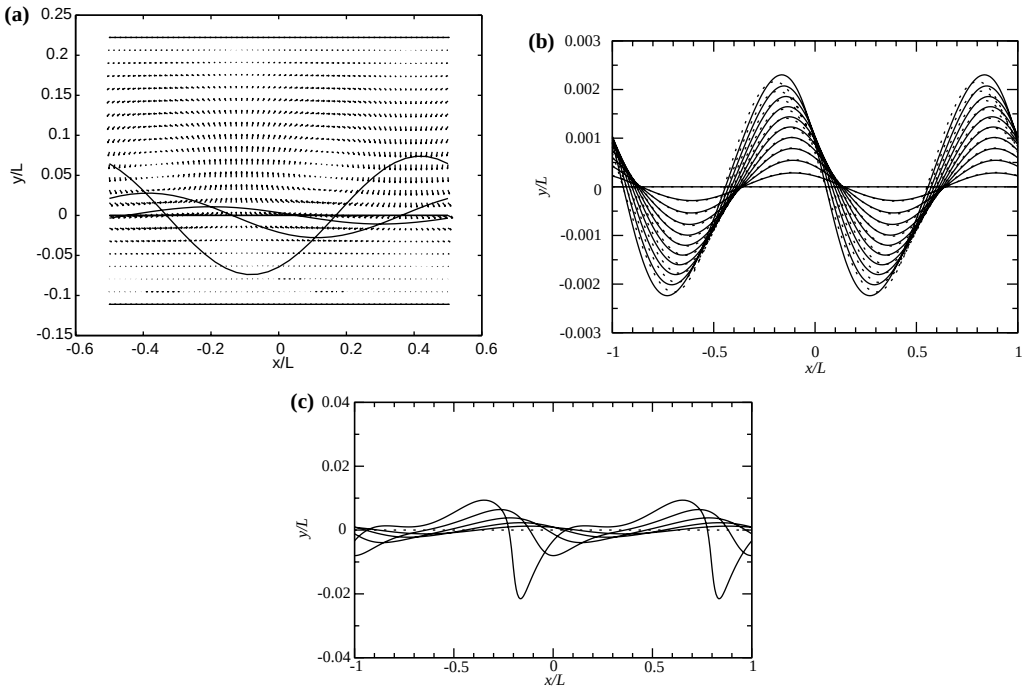

Figure 9. (*a*) Structure of the two-mode perturbation for a flat interface, and illustration of the linear growth of the interface for $r=2$, $\lambda=1$, $\mathrm{Ca}=2$, $\mathrm{Re}=1{\cdot}333$, and $\mathrm{Ma}=1{\cdot}0$. (*b*) Comparison between the results of the numerical simulation (solid lines) and predictions of linear theory (broken lines), Profiles are shown at times t = 0 (flat), 1, 2, ... (*c*) Interface profiles at times t = 0 (flat), 1, 5, 10, ..., showing the large deformation.

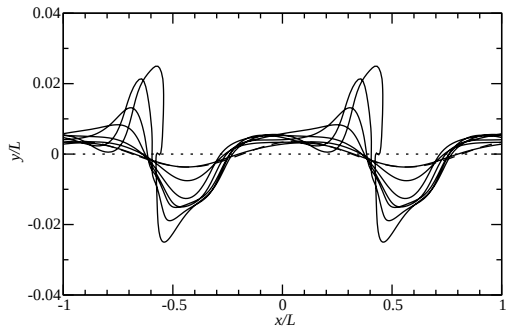

Figure 10. Growing interfacial waves due to the combined Yih-Marangoni instability for $r=1{\cdot}5$, $\lambda=0{\cdot}5$, $\mathrm{Ca}=2$, $\mathrm{Re}=10{\cdot}0$, $\mathrm{Ma}=1{\cdot}0$, at times t = 0 (flat interface), 1, 2, ... The dashed line represents the predictions of linear theory at $t=1{\cdot}0$.

Similar results are obtained for different flow conditions. For example, Figure 10 illustrates evolving interfacial profiles for $r=1{\cdot}5$, $\lambda=0{\cdot}5$, $\mathrm{Ca}=2$, $\mathrm{Re}=10{\cdot}0$, and $\mathrm{Ma}=1{\cdot}0$, and a perturbation with wave number $k=1{\cdot}0$. Note that, in this figure, x and y are dimensional variables reduced by the disturbance wave length L. Under these conditions, the Yih and Marangoni modes grow with respective dimensionless rates $-0{\cdot}47993$ and $0{\cdot}19655$, and travel with different phase velocities. In this simulation, the initial amplitude in the surfactant concentration is $0{\cdot}5$. The dashed line represents the predictions of linear theory at $t=1{\cdot}0$, which is in excellent agreement with the results of the simulation. As the amplitude of the interface grows, the crests of the developing waves tend to steepen and eventually overturn.

6. Discussion

The effect of inertia on the instability of the two-layer, shear-driven channel flow with a surfactant-laden interface was investigated by a linear stability analysis. Equal-density fluids have been considered in order to isolate the effects of the viscosity stratification and the induced Marangoni forces at the interface. In the event of small interfacial deflections, the evolution of normal-mode perturbations is governed by a two-fluid generalization of the Orr–Sommerfeld equation. Yih [13] demonstrated that, for a clean interface in the absence of surfactant, arbitrarily small inertia is sufficient to destabilize the flow. With both inertia and surfactant present, Marangoni forces act either to destabilize the flow, or else to significantly lower the decay rate of infinitesimal disturbances.

In the first part of this work, we conducted a numerical investigation of the Orr–Sommerfeld equation using the Chebyschev tau method, and computed growth rates for arbitrary wave numbers and Reynolds numbers. The results obtained for a clean interface agree with those previously given by Yih [13] and Renardy [14]. When surfactant is present, the Yih mode dominates the instability at small wave numbers, while the Marangoni mode controls the instability at moderate to large wave numbers. Neutral stability curves plotted at sample parameter values show that, for Reynolds numbers lower than a critical value, a range of small wave numbers subtended from zero exists with positive growth rates, corresponding to instability. Beyond the critical Reynolds number, a slender island of stable modes appears covering small to moderate wave numbers. By raising the viscosity contrast between the two fluids, a dramatic change in the topology of the neutral curve occurs, leaving a large hoop of unstable modes covering a wide area of parameter space, and a small pool of unstable modes encompassing the origin. As the viscosity contrast is raised further, the small pool shrinks towards the origin and eventually disappears.

In the second part of this work, the nonlinear evolution of the interfacial waves has been examined by numerical methods. Recently, Blyth and Pozrikidis [5] used a boundary-element method to conduct simulations for waves of finite-amplitude under conditions of Stokes flow, and demonstrated nonlinear saturation and the occurrence of wave overturning. In the presence of inertia, we have followed the nonlinear evolution of finite-amplitude interfacial waves numerically using a combination of Peskin's immersed-interface method and the diffuse-interface approximation. Trial simulations provided excellent agreement with the predictions of the linear theory during the early stages of the evolution. As nonlinear effects come into play, the interfacial waves begin to steepen and develop characteristic saw-tooth profiles. Eventually the waves overturn and are expected to break.

The present results emphasize the important role played by inertia in determining the stability of the two-layer flow when Marangoni forces are active. Increased inertia widens the range of unstable wave numbers, and makes the flow more susceptible to linear instability. This may lead to nonlinear growth and ultimately to wave breaking. However, increasing the level of inertia also opens a narrow window of stable modes of large wave length, and so in this sense provides a stabilizing effect. In the event of fluid layers of equal thicknesses, a small amount of inertia destabilizes the system immediately.

The stability characteristics at high Reynolds number have not been examined in detail. When the viscosity ratio is high, the hoop of unstable wave numbers subtended from a critical Reynolds number is reminiscent of those encountered in more classical parallel flow studies. Our numerical results suggest that the upper branch does not approach the horizontal axis as the Reynolds number is raised. For increasing Reynolds number, the range of unstable wave numbers may widen indefinitely, or begin to shrink; in fact, the upper branch may even attach

to the lower branch to form a closed loop. A boundary layer analysis combined with a more thorough numerical investigation at large Reynolds number would prove useful in addressing these questions.

Acknowledgement

Support for this research was provided by the National Science Foundation.

References

1. C. Pozrikidis, Effect of inertia on the Marangoni instability of two-layer channel flow, Part I: numerical simulations. *J. Engng. Math.* 50 (2004) 311–327.
2. C. Pozrikidis, Instability of multi-layer channel and film flows. *Adv. Appl. Mech.* 40 (2004) In press.
3. A.L. Frenkel and D. Halpern, Stokes-flow instability due to interfacial surfactant. *Phys. Fluids.* 14 (2002) 45–48.
4. D. Halpern and A.L. Frenkel, Destabilization of a creeping flow by interfacial surfactant: linear theory extended to all wave numbers. *J. Fluid Mech.* 485 (2003) 191–220.
5. M.G. Blyth and C. Pozrikidis, Effect of surfactants on the stability of two-layer channel flow. *J. Fluid Mech.* 505 (2004) 59–86.
6. X. Li and C. Pozrikidis, The effect of surfactants on drop deformation and on the rheology of dilute emulsions in Stokes flow. *J. Fluid Mech.* 341 (1997) 165–194.
7. S. Yon and C. Pozrikidis, A finite-volume/boundary-element method for flow past interfaces in the presence of surfactants, with application to shear flow past a viscous drop. *Comput. Fluids.* 27 (1998) 879–902.
8. S.A. Orszag, Accurate solution of the Orr–Sommerfeld stability equation. *J. Fluid Mech.* 50 (1971) 689–703.
9. J.J. Dongarra, B. Straughan and D.W. Walker, Chebyshev tau-QZ algorithm methods for calculating spectra of hydrodynamic stability problems. *Appl. Num. Math.* 22 (1996) 399–434.
10. D. Gottlieb and S.A. Orszag, *Numerical Analysis of Spectral Methods.* Philadelphia: SIAM (1977) 172 pp.
11. A.P. Gallagher and A.McD. Mercer, On the behaviour of small disturbances in plane Couette flow. *J. Fluid Mech.* 13 (1962) 91–100.
12. C. Pozrikidis, *Introduction to Theoretical and Computational Fluid Dynamics.* New York: Oxford University Press (1997) 675 pp.
13. C.S. Yih, Instability due to viscosity stratification. *J. Fluid Mech.* 27 (1967) 337–352.
14. Y. Renardy, Instability at the interface between two shearing fluids in a channel. *Phys. Fluids.* 29 (1985) 3441–3443.
15. A.P. Hooper and W.G.C. Boyd, Shear-flow instability at the interface between two viscous fluids. *J. Fluid Mech.* 128 (1983) 507–528.